The Journal of Chemical Physics

A grand canonical Monte Carlo study of SO_2 capture using functionalized bilayer graphene nanoribbons

Cite as: J. Chem. Phys. **146**, 044704 (2017); https://doi.org/10.1063/1.4974309
Submitted: 26 September 2016 . Accepted: 05 January 2017 . Published Online: 26 January 2017

Manish Maurya, and Jayant K. Singh

A grand canonical Monte Carlo study of SO_2 capture using functionalized bilayer graphene nanoribbons

Manish Maurya and Jayant K. Singh[a)]
Department of Chemical Engineering, Indian Institute of Technology Kanpur, Kanpur 208016, India

(Received 26 September 2016; accepted 5 January 2017; published online 26 January 2017)

Grand canonical Monte Carlo (GCMC) simulation is used to study the adsorption of pure SO_2 using a functionalized bilayer graphene nanoribbon (GNR) at 303 K. The functional groups considered in this work are OH, COOH, NH_2, NO_2, and CH_3. The mole percent of functionalization considered in this work is in the range of 3.125%–6.25%. GCMC simulation is further used to study the selective adsorption of SO_2 from binary and ternary mixtures of SO_2, CO_2, and N_2, of variable composition using the functionalized bilayer graphene nanoribbon at 303 K. This study shows that the adsorption and selectivity of SO_2 increase after the functionalization of the nanoribbon compared to the hydrogen terminated nanoribbon. The order of adsorption capacity and selectivity of the functionalized nanoribbon is found to follow the order COOH > NO_2 > NH_2 > CH_3 > OH > H. The selectivity of SO_2 is found to be maximum at a pressure less than 0.2 bar. Furthermore, SO_2 selectivity and adsorption capacity decrease with increase in the molar ratio of SO_2/N_2 mixture from 1:1 to 1:9. In the case of ternary mixture of SO_2, CO_2, N_2, having compositions of 0.05, 0.15, 0.8, the selectivity of SO_2 over N_2 is higher than that of CO_2 over N_2. The maximum selectivity of SO_2 over CO_2 is observed for the COOH functionalized GNR followed by NO_2 and other functionalized GNRs. *Published by AIP Publishing.* [http://dx.doi.org/10.1063/1.4974309]

I. INTRODUCTION

Emission of acidic gases such as CO_2 and SO_2 due to the burning of fossil fuels has become an environmental and health hazard. Recently, sequestration of CO_2 from flue gas, to curtail the greenhouse gas effect, has drawn unprecedented attention.[1–3] On the other hand, SO_2 being one of the most harmful gases arising mostly from flue gas is equally hazardous, and therefore it also needs to be captured. Emission of SO_2 causes acid rain which has a detrimental effect on the fertility of soil and walls of buildings and monuments. Moreover, it can adversely affect the respiratory systems. Therefore, controlling its emission has become increasingly urgent for environment and human health. Removal of SO_2 from flue gas can be categorized into either dry or wet recovery.[4] Conventionally, flue gas desulfurization is accomplished by an absorption process, such as ammonia scrubbing, limestone scrubbing, and organic solvent absorption.[5–7] Amine solutions, such as ethylenediamine and amino acids, are also reported to be efficient for flue gas desulfurization.[8,9] However, these conventional methods have some inherent disadvantages like, generation of secondary pollutants, loss of solvents, large amount of water, and excessive energy consumption for regeneration.[10] Recently, azole based ionic liquids have also shown great potential for flue gas desulfurization due to their high thermal stability and tunable properties.[11,12] Adsorption process provides an alternative and promising technology for emission control of SO_2 from flue gas. Compared to the absorption process, adsorption process is relatively simple and less energy intensive without any byproduct. Since the partial pressure of SO_2 is very low in flue gas, the promising adsorbent should have high capacity at ambient conditions. Hence, to capture SO_2 efficiently, the quest of better adsorbent is warranted. In order to understand the mechanism of SO_2 adsorption, numerous adsorbents have been reported in the literature, including activated carbons,[13,14] carbon nanotubes (CNTs),[15,16] zeolites,[17,18] supported polymers,[19] carbon fibers,[20,21] and more recently metal-organic frameworks.[22,23]

Among these adsorbents, carbon based adsorbents have shown better affinity towards SO_2. Although zeolite and metal organic frameworks have high micropore volume resulting in high capacity, most of them are not stable under humid conditions. Due to its better stability under such conditions, carbonaceous materials are more appealing than the framework materials. In addition, functional groups at the surface of activated carbons, which consists of edge functionalized broken graphene sheets, can positively influence the adsorption capacity of an adsorbent.[24] Thus, there are techniques, which are used frequently in the literature to enhance the material adsorption capacity such as the fabrication of new porous materials and incorporation of functional groups to the surface of the material.[25–29] Recently, graphene, a one-atom thick 2-D layer of graphite, has been synthesized by Novoselov *et al.*[30] This has resulted in extensive investigations on graphene based structures in various fields of research due to its unique physical property and applications.[31] Numerous gas adsorption studies using graphene surface have been reported recently,[32,33] which show that gas molecules such as NO_2, CO_2, and NH_3 can get physically adsorbed on pristine graphene. Graphene nanoribbon can also be used as a chemical sensor for certain gases such as NH_3.[34] However, the

a)Electronic mail: jayantks@iitk.ac.in

adsorption efficiency of graphene based materials for SO_2 adsorption has not been studied to the best of our knowledge. Grand canonical Monte Carlo (GCMC) based computer simulation is one of the common methods to understand the adsorption behaviour of gases in porous materials. Several adsorption studies of CO_2, CH_4, H_2, and N_2 on different porous materials have been reported using GCMC simulations.[35–39] This method is successfully used to predict the capacity of a porous material to store energy gases such as methane and hydrogen under different conditions.[40–43] In this study, we have used GCMC simulation to investigate the effect of edge functionalization in bilayer graphene nanoribbons (GNRs) on separation of SO_2 from binary and ternary mixtures of SO_2, CO_2, and N_2. The following acidic and basic functional groups are considered in this work: OH, NH_2, CH_3, COOH, and NO_2. Thus, the motivation of this work is to find out the effect of functionalization on the adsorption capacity and selectivity of the GNR.

II. MODELS AND METHODS

A. Potential models

In this work, three-site rigid models of Potoff *et al.* are used to represent sulfur dioxide, carbon dioxide, and nitrogen molecules.[44,45] In these models, charges are located at each site. The potential parameters and procedure to functionalize the GNR are taken from Dasgupta *et al.*[46] The process of functionalization is discussed in Sec. II B. The authors have found that the classical parameters for functionalized graphene capture the effective interactions with the adsorbates accurately. Furthermore, orientation of adsorbates obtained from the classical forcefield is also in close agreement with the optimized orientation using the density functional theory. In the course of simulations, the adsorbate and adsorbent are considered to be rigid with frozen atoms, i.e., during translation and rotation moves, the bond length and bond angle of adsorbate molecules are kept fixed. The interaction energy between two pairs of molecules is expressed as the sum of Lennard-Jones (LJ) and Coulombic interactions as follows:

$$E = \sum_{ij} 4\epsilon_{ij}\left[\left(\frac{\sigma_{ij}}{r_{ij}}\right)^{12} - \left(\frac{\sigma_{ij}}{r_{ij}}\right)^{6}\right] + \sum_{ij}\frac{Cq_iq_j}{\epsilon r_{ij}}, \quad (1)$$

where r_{ij} and σ_{ij} are distance between sites i and j of two molecules and the distance at which cross LJ interaction potential is zero, respectively. ϵ_{ij} is the energy parameter between two sites of a molecule, and q_i and q_j are charges on site i and site j of two molecules, respectively. All the interactions between fluid-fluid and fluid-solid molecules are calculated site-wise, whereas cross interaction energy parameters are approximated using Lorentz-Berthelot rules (i.e., $\epsilon_{ij} = (\epsilon_{ii}\epsilon_{ij})^{1/2}$ and $\sigma_{ij} = (\sigma_{ii} + \sigma_{jj})/2$).[47] All the energy and size parameters of the adsorbate and adsorbent are listed in Tables I and II, respectively.

B. Simulation details

Fig. 1 shows the snapshot of the bilayer GNR in AB stacking which is used in this work. In AB stacking, carbon atoms in the top layer is at the center of the hexagon formed by carbon atoms of the lower layer and this arrangement is more stable than other stackings.[48] There are 192 carbon atoms in each sheet having a stacking distance of 3.34 Å.[46] The bond length between the two carbon atoms in the layer is 1.42 Å. The GNR is considered as a hydrogen terminated nanoribbon of graphene. In order to study the effect of different functional groups on the adsorption behavior of SO_2, hydrogen terminated edges of each graphene nanoribbons are replaced by aforementioned functional groups, alternatively. Simulations are performed for two different concentrations (by mole) of functional groups, viz., 3.125% and 6.25%. The former results in a total of 12 functional groups in the system having 6 functional groups at the edges of each sheet. On the other hand, in the latter case there are totally 24 functional groups in the system having 12 groups at the edges of each sheet. A graphene nanoribbon of width 15 Å is made periodic in the y direction only and it is placed parallel to the x-y plane in the simulation box. The box dimension in the x and z directions is taken large enough to avoid the effect of its periodic images on the adsorption phenomenon. The simulation box dimensions that we have

TABLE I. Force field parameters for SO_2 and N_2 molecules.[44,45]

Atom	σ (Å)	ϵ (kcal/mol)	q (e)
S	3.39	0.147	0.59
O	3.05	0.157	−0.295
N	3.31	0.072	−0.482
N (COM)	0.0	0.0	0.964

TABLE II. Force field parameters for graphene and functional groups, where C^e is the carbon atom of graphene which is attached to the functional group. O^a is the oxygen atom which is connected to carbon with double bond whereas O^b is connected to carbon and hydrogen via single bond.[46]

Functional group	Atom	σ (Å)	ϵ (kcal/mol)	q (e)
Graphene	C	3.4	0.056	0.0
H	C^e	3.55	0.07	−0.115
	H	2.42	0.030	0.115
OH	C^e	3.55	0.07	0.15
	O	3.07	0.17	−0.585
	H	0.0	0.0	0.435
NH_2	C^e	3.55	0.07	0.18
	N	3.3	0.17	−0.9
	H	0.0	0.0	0.36
NO_2	C^e	3.55	0.07	0.09
	N	3.25	0.12	0.65
	O	2.96	0.17	−0.37
CH_3	C^e	3.55	0.07	−0.115
	C	3.5	0.066	−0.065
	H	2.5	0.030	0.06
COOH	C^e	3.55	0.07	0.0
	C	3.75	0.105	0.468
	O^a	2.96	0.21	−0.396
	O^b	3.0	0.17	−0.477
	H	0.0	0.0	0.405

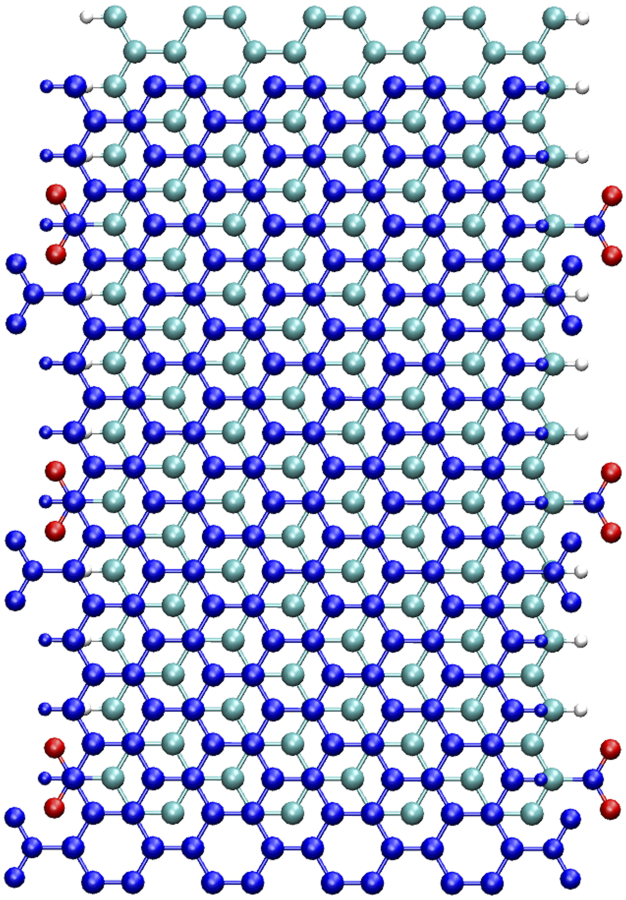

FIG. 1. Snapshot of functionalized graphene nanoribbon. Blue and cyan colours represent top and bottom layers. Edges are terminated with either hydrogen or functional groups.

taken are L_x = 100 Å, L_y = 29.5 Å, and L_z = 100 Å. GCMC simulations of the adsorption of pure SO_2 on edge functionalized bilayer graphene nanoribbons are performed at 303 K using different chemical potentials to generate the adsorption isotherm up to a pressure of 2.5 bars. The Widom insertion method is used to calculate the values of the chemical potential of gases in the bulk phase at different concentrations. In the case of binary mixtures, two different concentrations are considered, 1:1 and 1:9 mole ratios, whereas the concentration of ternary mixtures of SO_2, CO_2, and N_2 gases are 0.05, 0.15, and 0.8 mole ratios, respectively. Three Monte Carlo moves are used, viz., displacement, addition/deletion, and rotation with different probabilities of 0.2, 0.7, and 0.1, respectively. In addition, identity swap move is used for mixture simulations. It should be noted that the frequency of the different MC moves do not influence the final result but they control the efficiency of the exploration of configuration space and they must be adequately matched to the type of simulation considered. There is no general rule of selecting optimal frequencies. Nevertheless, few guidelines suggest that the total number of accepted transfer moves (addition/deletion) is at least one tenth of the accepted internal moves (translations, rotations, . . .).[49,50] All simulations in this work are performed using in-house Monte Carlo code written in C++. This code is validated by matching fluid properties with NIST[51] data and has been used to study gas adsorption in a porous material.[28] Each simulation consists of equilibration and production run of 5×10^7 MC steps. Non bonded interactions are accounted using the Ewald summation method. A cutoff distance of 14.7 Å is used for both Coulombic and LJ interactions. The results presented in this work do not change upon increasing the system size, which is verified by conducting additional simulations for a larger system size (twice the original size of the GNR).

C. Adsorption theory

In GCMC simulations, at a constant T, V, and μ, we get the absolute number of adsorbed particles (N_{ad}) in the simulation box. However, experimentally obtained data are in the excess amount of adsorption (N_{excess}). Thus, we have converted absolute adsorption into excess adsorption using the following expression:

$$N_{excess} = N_{ad} - \rho_b V_{free}, \tag{2}$$

where ρ_b is the bulk density of the adsorbate which is obtained from independent GCMC simulation at the same thermodynamic conditions and V_{free} is the accessible volume for the fluid molecules. There exist several methods to calculate the accessible volume.[52–54] In this work, free volume is calculated using a helium adsorption technique.[54] In addition to the excess adsorption data, a thermodynamic quantity of interest is the isosteric heat of adsorption, which reflects the amount of heat liberated while adding each molecule in the adsorbed phase. In other words, isosteric heat is a measure of interaction strength between the adsorbate and adsorbent molecules which is approximated by[55]

$$q_{st} \approx RT - \left(\frac{\partial U_{ad}}{\partial N_{ad}}\right)_{T,V}, \tag{3}$$

where U_{ad} is the total energy of the adsorbed phase. The partial derivative in the above expression is calculated using the fluctuation theory. The resultant expression for the isosteric heat of adsorption is as follows:[56]

$$q_{st} = RT - \frac{\langle U_{ad} N_{ad}\rangle - \langle U_{ad}\rangle\langle N_{ad}\rangle}{\langle N_{ad}^2\rangle - \langle N_{ad}\rangle^2}, \tag{4}$$

where angled brackets represent ensemble average. In a binary mixture, the selectivity of species i over j is defined as

$$S_{i/j} = \left(\frac{x_i}{x_j}\right)\left(\frac{y_j}{y_i}\right), \tag{5}$$

where x and y are the mole fractions of species in adsorbed and bulk phases, respectively.

III. RESULTS AND DISCUSSION

A. Pure SO_2 adsorption isotherms on functionalized GNR

Fig. 2 shows the excess SO_2 adsorption isotherms for 3.125% and 6.25% functionalized GNRs with different functional groups at 303 K. The amount of excess adsorption increases with pressure for all the functional groups. This behavior is seen for both the percentages of functionalization. It can be seen that after the functionalization of the nanoribbon, its gas uptake capacity increases compared to the hydrogen terminated GNR. Among all the functional groups,

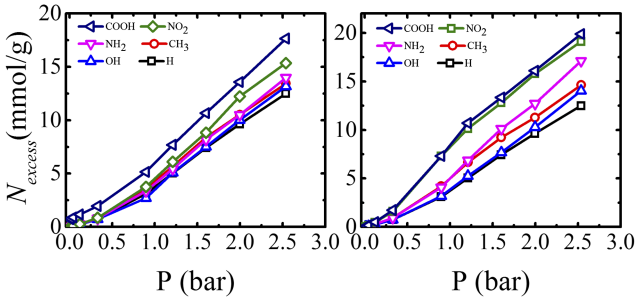

FIG. 2. Excess adsorption isotherms of SO_2 in 3.125% (left) and 6.25% (right) functionalized GNRs using different functional groups at 303 K.

maximum excess uptake is observed for COOH followed by NO_2 and other functional groups for both the percentages of functionalization. At 1 bar and 303 K, the excess uptake for the 6.25% COOH functionalized GNR is ≈8 mmol/g, which is the maximum among all functional groups studied in this work. In a recent experimental work, graphene oxide (specific surface area 268 m^2/g) was shown to have SO_2 capacity of ≈2.5 mmol/g at 298 K and 1 bar,[57] whereas most of the activated carbons have experimentally observed uptake of SO_2 less than 6 mmol/g[14,58] at similar conditions. In the current study, adsorption capacities of the OH terminated GNR for 3.125% and 6.25% functionalizations at 1 bar are found to be ≈2.5 and 2.7 mmol/g, respectively. Thus, theoretical estimate of the adsorption capacity of the GNR with OH termination shows a similar capacity at low pressures as seen in experiments by Babu *et al.*[57] and Grzyb *et al.*[14] for graphene oxide and activated carbon, respectively. However, the values differ significantly at high pressures for both percentages of functionalization, which is due to the large specific surface area (1176 m^2/g) of the nanoribbon considered in this work. It should be noted that graphene oxide considered in the aforementioned work of Babu *et al.*[57] contains more than two layers of graphene sheet leading to decrease in the surface area per unit mass of the adsorbent. Thus, the graphene oxide considered in this work is more idealized. In the case of pristine graphene, the adsorption is physisorption and the charge transfer between the graphene and adsorbate is almost negligible. A vacancy in the graphene sheet may provide (physisorption/chemisorption) binding sites for the adsorbate, thus increasing the amount of adsorption as reported in recent works.[59,60] The adsorption capacity of carbon material has been recently studied for SO_2 gas, particularly on carbon nanotubes using GCMC simulations. For example, it has been shown by Wang *et al.*[15] that the adsorption capacity of SO_2 in an array of single wall carbon nanotubes is ≈15 mmol/g at 1 bar and 303 K. In another

TABLE III. Henry's adsorption constant for 3.125% (left) and 6.25% (right) functionalized GNRs. R^2 is the coefficient of determination of fitted data.

Group	K_H (mmol/g bar)	R^2	K_H (mmol/g bar)	R^2
H	3.304	0.978	3.304	0.978
CH_3	3.769	0.975	4.419	0.971
OH	2.905	0.985	3.377	0.974
NH_2	3.552	0.975	4.322	0.973
NO_2	3.959	0.972	7.676	0.968
COOH	5.871	0.897	7.731	0.974

TABLE IV. Freundlich isotherm parameters obtained by fitting SO_2 adsorption data on the 6.25% functionalized GNR. R^2 is the coefficient of determination of fitted data.

Functional group	ln(K)	1/n	R^2
H	1.329	1.188	0.995
CH_3	1.547	1.192	0.996
OH	1.371	1.203	0.994
NH_2	1.608	1.209	0.995
NO_2	1.946	1.21	0.998
COOH	1.983	1.167	0.997

study, Rahimi *et al.*[16] have shown a SO_2 adsorption capacity of 14 mmol/g at the same condition in an array of double wall carbon nanotubes (specific surface area ≈1282 m^2/g) using an intertube distance and a diameter of 1 nm and 3 nm, respectively. High adsorption capacity in these materials is mainly because of the high specific surface area and confinement effects. It is noted that the temperature effect is not reported in this work. However, we expect the adsorption amount of SO_2 on GNRs to decrease at higher temperatures as reported by various workers.[61,62] Since physisorption is an exothermic process, according to Le Chatelier's principle,[63] the amount of adsorption must decrease with increase in temperature.

In order to ascertain the strength of adsorption of GNRs at low pressures, we have obtained the Henry's adsorption constants, which are listed in Table III. The table shows that the Henry's adsorption constant increases with increase in the percentage of functionalization, indicating improved adsorption capacity. In order to understand the adsorption behaviour on the GNR, the Freundlich model is used,[64]

$$N_{excess} = K_H P^{1/n}, \tag{6}$$

where $1/n$ represents the intensity of adsorption and K_H is the Freundlich constant, which shows the capacity of adsorption. The Freundlich adsorption model has been fitted to the entire SO_2 adsorption data for 6.25% functionalization. Table IV summarizes the fitted model parameters. It is observed that isotherms for both the percentages of functionalization follow the Freundlich model. Significant enhancement in adsorption capacity for COOH and NO_2 functionalized GNRs from the hydrogen terminated GNR can be attributed to the significant dipole-dipole interactions with the fluid molecule as they possess a high dipole moment

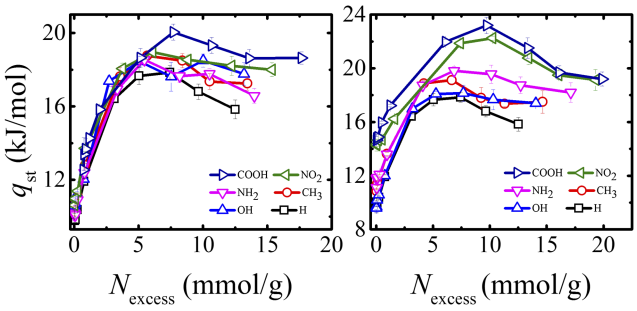

FIG. 3. Isosteric heat of SO_2 adsorption in 3.125% (left) and 6.25% (right) functionalized GNRs using different functional groups.

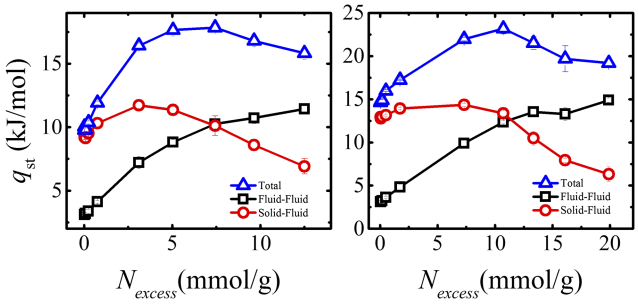

FIG. 4. Figure shows the contribution of fluid-fluid and fluid-solid heat of adsorption to the total heat for hydrogen (left) and carboxyl (right) group terminated GNRs.

compared to other functional groups. Apart from the dipole-dipole interaction, Lewis acid and Lewis base interactions also play an important role in the adsorption behavior of SO_2.

The effect of functional groups is also reflected in the heat of adsorption data as shown in Fig. 3. The maximum heat of adsorption follows the order of adsorption amount observed for various functional groups: COOH > NO_2 > NH_2 > CH_3 > OH > H, for both percentages of functionalization. Since each functionalized surface has different excess adsorption at a given pressure, the maximum heat of adsorption for various functionalized GNRs occurs at different values of excess adsorption. The non-monotonous behaviour of the isosteric heat can be attributed to the competitive nature of fluid-fluid and fluid-solid interactions. Fig. 4 shows the contribution of fluid-fluid and fluid-solid heat of adsorptions, along with the total heat of adsorption. Heat of adsorption for

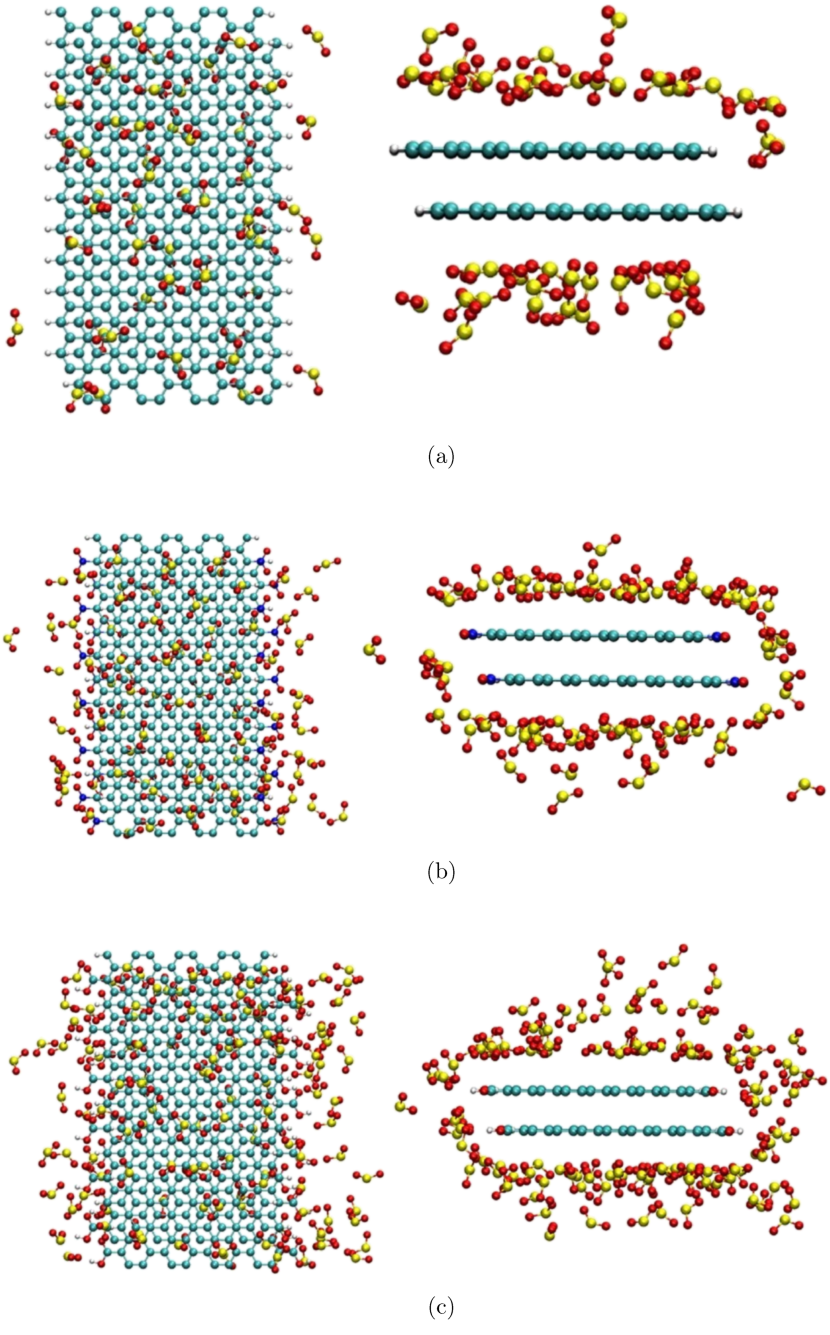

FIG. 5. Top and side views of SO_2 adsorption on the 6.25% functionalized GNR with (a) H, (b) NO_2, and (c) COOH functional groups at 1 bar.

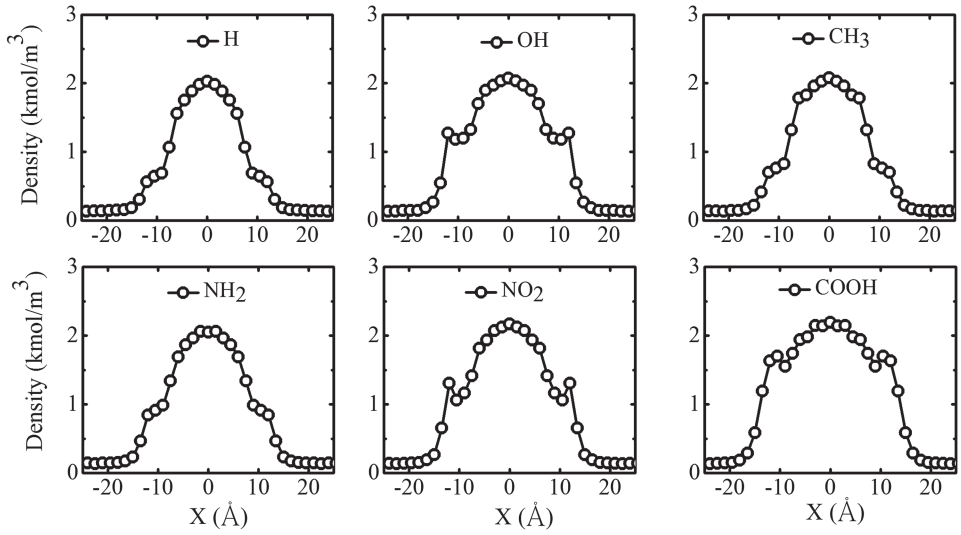

FIG. 6. Absolute density distribution of SO_2 along the width of the 3.125% functionalized nanoribbon at 1 bar, 303 K.

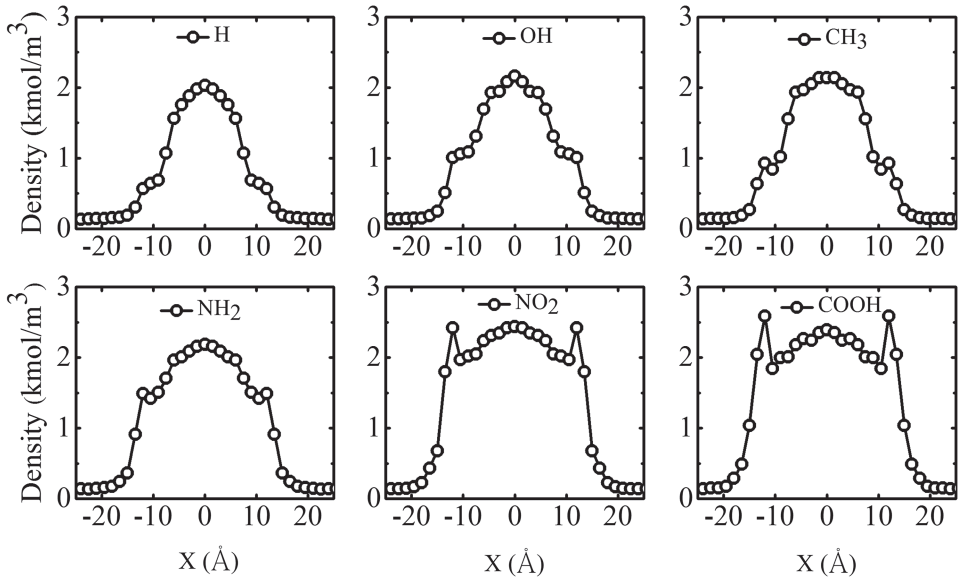

FIG. 7. Absolute density distribution of SO_2 along the width of the 6.25% functionalized nanoribbon at 1 bar, 303 K.

fluid-fluid and fluid-solid pairs are calculated using individual interaction energies of the pair with the help of Equation (4), whereas total interaction energy is used for calculating the total heat of adsorption. At a low loading, the fluid-solid interaction is significantly higher than that of the fluid-fluid interaction. Thus, the contribution of the fluid-solid heat of adsorption is much higher than that of the fluid-fluid. However, due to the increase in the surface coverage with loading, solid-fluid contribution to the heat of adsorption decreases. On the contrary, the contribution due to the fluid-fluid interaction increases with loading. At an intermediate excess adsorption, a crossover behavior is observed where the fluid-fluid contribution overtakes the solid-fluid contribution and is reflected in the maximum amount of the total heat of adsorption. This behavior is observed for all the functional groups. However, the excess adsorption at which the crossover occurs is dependent on the functional group. A strong or affable group tends to delay the crossover as observed for the COOH group (see Fig. 4). Adsorption of gas molecules occurs because of the excess energy of the adsorbent. Subsequent to the adsorption of gas molecules, surface excess energy of the adsorbent decreases with increasing coverage of the surface by the gas molecules. Hence solid-fluid interaction dominates at low loadings only. On the other hand, the fluid-fluid interaction increases at higher adsorption because of greater contribution from the neighboring adsorbed molecules owing to increase in the number of molecules at a high pressure.

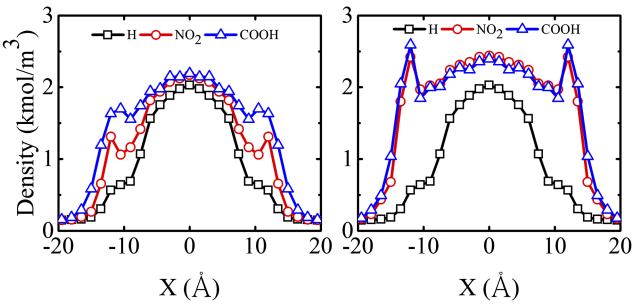

FIG. 8. Comparison of absolute density distribution at 1 bar across 3.125% (left) and 6.25% (right) functionalized GNRs, respectively.

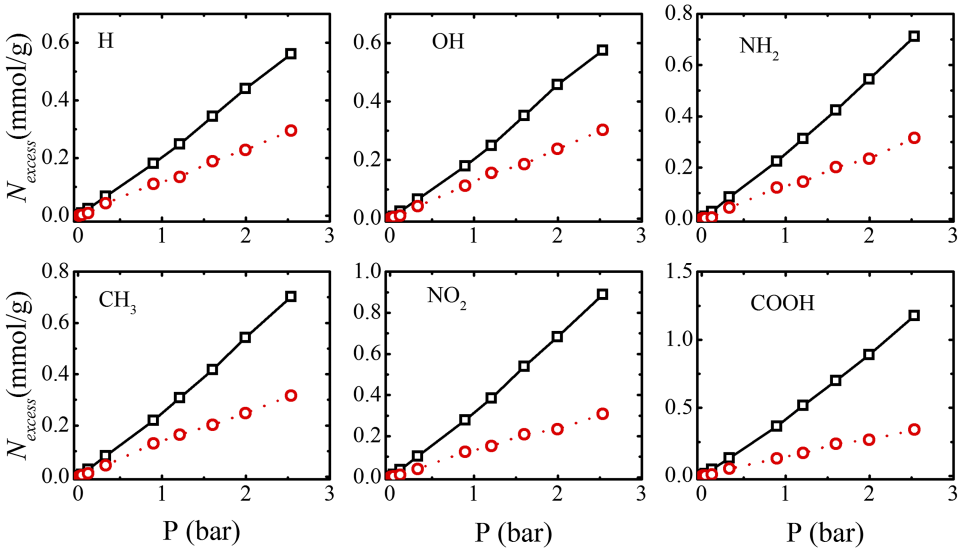

FIG. 9. Excess adsorption isotherms of the equimolar mixture of SO_2/N_2 in the 6.25% functionalized GNR using different functional groups at 303 K. Dotted line is the representative of nitrogen adsorption in all the functional groups terminated GNR, which does not change significantly.

Fig. 5 presents the snapshots of SO_2 adsorption for the 6.25% functionalized GNR at 1 bar. The snapshots show adsorption on the functionalized GNR, where the edge effect can be seen around functional groups other than the H terminated GNR. In the case of the hydrogen terminated GNR, adsorption of SO_2 occurs only at the top of the surface. On the other hand, other functional groups terminated GNRs, owing to its polarity, show adsorption not only on the top of the GNR but also around the edge of the GNR. As we increase the percentage of functionalization on the GNR, the density distribution increases around COOH, NO_2, and OH functional groups. On the other hand, for H, CH_3, and NH_2 functional groups very small enhancement in the density is observed around the functional groups as seen in Figs. 6 and 7. Snapshots of SO_2 adsorption on CH_3, NH_2, and OH functionalized GNRs are given in Fig. S1 of the supplementary material. The density distribution along the width of the nanoribbon is calculated by the averaging adsorbed number of particles in the y and z directions. In the case of 3.125% functionalization, the distribution peak around functional groups is slightly pronounced compared to the hydrogen terminated graphene nanoribbon. These density peaks are stepped up remarkably at 6.25% functionalization compared to 3.125% functionalization, especially in the case of COOH and NO_2 functional groups as seen in Fig. 8. This trend of adsorption density distribution with different functional groups can be attributed to the dipole moment of these functional groups. The experimental dipole moments of NO_2, OH, NH_2, CH_3, and COOH are 4.22, 1.224, 1.53, 0.332, and 1.72 D, respectively.[65] SO_2 having a high dipole moment (1.6 D) interacts strongly with these functional groups terminated GNRs compared to the hydrogen terminated GNR, thus demonstrating better adsorption capacity. In the case of the COOH functional group, the presence of a ketonic group enhances the interaction because of strong Lewis acid and base interactions. Thus, increase in the amount of the functional group in the system produces a stronger interaction, causing improved adsorption capacity.

B. SO_2/N_2 mixture adsorption isotherms on functionalized GNR

Considering that the flue gas contains a mixture of various gases mostly N_2 along with SO_2 in ppm concentration, we turn our attention towards understanding the adsorption of SO_2 using the GNR from the flue gas mixture. In this work, we have treated flue gas as a binary mixture of SO_2 and N_2 having SO_2/N_2 concentrations of 1:1 and 1:9 mole ratios. Fig. 9 shows the equimolar mixture adsorption isotherm of SO_2 and N_2 in the 6.25% functionalized GNR. It is observed that the excess adsorption of SO_2 follows the same behaviour as in the pure component adsorption. The adsorption capacity of SO_2 in COOH functionalization of the GNR is the highest followed by the NO_2 functional group. At 1 bar partial pressure of SO_2, the adsorption capacity of SO_2 in SO_2/N_2 mixture for the COOH functionalized GNR is 0.8 mmol/g, which is less than the pure component adsorption of SO_2 by 90%. The adsorption capacities of SO_2 for NH_2 and CH_3 functionalized GNRs are almost similar in the studied range of pressure. It is evident from Fig. 9 that the adsorption behaviour of nitrogen is insensitive to functional groups. In fact, the adsorption isotherm of nitrogen overlaps for GNR functionalized with different functional groups (figure not shown). Fig. 10 shows that with increase in the nitrogen concentration, for the case

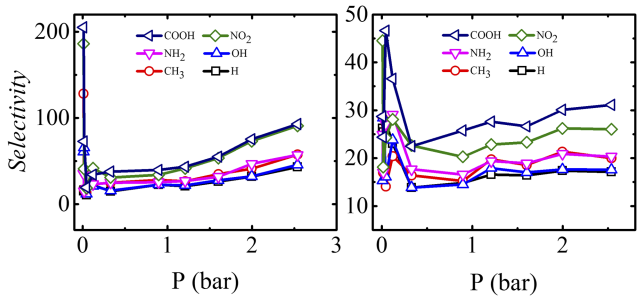

FIG. 10. Selectivity of SO_2/N_2 mixture for 1:1 (left) and 1:9 (right) mole ratios in the 6.25% functionalized GNR using different functional groups at 303 K.

of 1:9 mole ratio of SO_2/N_2 mixture, the selectivity of sulfur dioxide decreases. The selectivity of sulfur dioxide gas at 1 bar pressure in the mixture of 1:1 mole ratio is 40, whereas it falls below 30 for the mixture of 1:9 mole ratio for the COOH functional group. It is also obvious that the interaction of nitrogen with the surface is very low compared to SO_2. At a very low pressure, 0.01 bar, capacity of nitrogen is extremely small resulting in a spike in the selectivity. As we increase the pressure, nitrogen adsorption increases which reduces the selectivity and it remains almost constant till the pressure of 1.5 bars for the equimolar mixture. As the pressure is increased further towards the saturation pressure of SO_2, the capacity of SO_2 increases rapidly, so does the selectivity. This behaviour is obtained for the equimolar mixture only. The selectivity of SO_2 in 1:9 mixture concentration at a low pressure is high but it is less than the selectivity observed for the case of equimolar mixture. Moreover, selectivity drops as the pressure increases till 0.4 bar. When the pressure increases from 0.4 to 2 bars, selectivity increases, beyond that it becomes almost constant. Despite having high concentrations of N_2, its selectivity is low because of a very high vapour pressure compared to SO_2. Moreover, the dipole-dipole interaction of SO_2 is stronger than the quadrupole interaction of nitrogen with the GNR. Enhancement in density around the functional groups can be seen from the configurational snapshots of SO_2/N_2 mixture in Fig. 11. It is evident from the snapshot that SO_2 is being adsorbed more preferably on the surface. There is almost no effect of surface functionalization on the adsorption behaviour of nitrogen. Selectivities of COOH and NO_2 functionalized graphene are the highest among other functional groups for both the mixture concentrations.

C. $SO_2/CO_2/N_2$ mixture adsorption selectivity on functionalized GNR

In this section, we have extended the study of adsorption of a ternary mixture ($SO_2/CO_2/N_2$) on functionalized GNRs. In order to imitate the realistic flue gas composition, we have taken 0.05, 0.15, and 0.80 molar ratios of SO_2, CO_2, and N_2 in the mixture, respectively. Fig. 12 presents the selectivity of SO_2 and CO_2 over other gases. The selectivity of SO_2 over CO_2 increases with increase in the partial pressure of SO_2. The selectivity of SO_2 over N_2 shows improvement as compared to that observed for the binary mixture of SO_2/N_2. Rahimi *et al.*[66] have also seen that the selectivity of SO_2/N_2 in a ternary mixture of $SO_2/CO_2/N_2$ is higher than that of a binary mixture using CNT bundle. Strong affinity of SO_2 and CO_2 towards the GNR compared to N_2, leads to increase in the selectivity. The selectivity of SO_2 in a ternary mixture on the CNT bundle is higher than that of the GNR. This difference can be attributed to the confinement effect in the CNT bundle. In the case of CO_2/N_2 mixture, the selectivity of CO_2 is almost constant within the studied range of the partial pressure of CO_2, which is inline with that observed by Dasgupta *et al.*[46] Snapshot of adsorption in a ternary mixture is given in

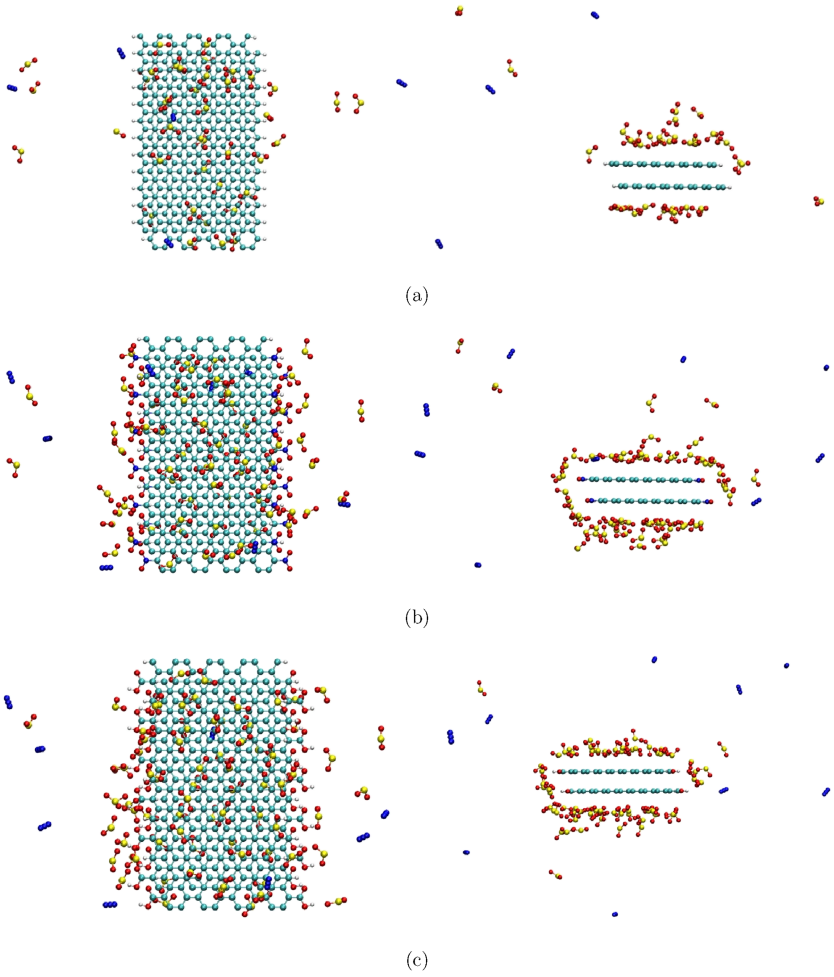

FIG. 11. Top and side views of equimolar SO_2/N_2 mixture adsorption on (a) H, (b) NO2, and (c) COOH terminated graphene nanoribbons at 1 bar. Blue colour represents N_2 while yellow along with red colour represent the SO_2 molecule.

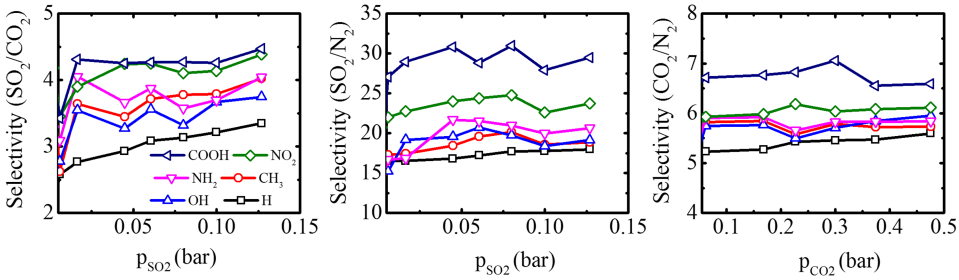

FIG. 12. Selectivity of $SO_2/CO_2/N_2$ mixture in the 6.25% functionalized GNR using different functional groups at 303 K.

Fig. S2 of the supplementary material. It is evident from Fig. 12 that the functionalized GNRs show better SO_2 selectivity for a ternary mixture in comparison with that of the hydrogen terminated GNR.

IV. CONCLUSIONS

In this study, we have considered the functionalized graphene nanoribbon as an adsorbent for sulfur dioxide adsorption. We have assessed the role of different functional groups and their concentrations (3.125%, 6.25 mol. %) on the adsorption of SO_2. First, we studied adsorption capacity of pure SO_2 on the GNR using GCMC simulations at 303 K then we determined the effect of functional groups on the selective adsorption of SO_2 in two different compositions (1:1 and 1:9 mole ratios) of SO_2/N_2 mixtures. Simulation results show that functionalization of the GNR enhances the SO_2 adsorption capacity compared to the hydrogen terminated GNR and it follows the adsorption order: COOH > NO_2 > NH_2 > CH_3 > OH > H functionalized GNR. This order of adsorption is observed for both percentage functionalizations of the GNR. The estimated adsorption capacity of SO_2 for the 6.25% COOH terminated GNR are 8 mmol/g and 20 mmol/g at 1 bar and 2.5 bars, respectively. The maximum adsorption strength of SO_2 for the functionalized GNR is also observed for the 6.25% COOH terminated GNR which is reflected in the heat of adsorption value of 23.2 kJ/mol. The selectivity of SO_2 in an equimolar mixture is maximum at a low pressure range, which decreases with increasing nitrogen concentration in the mixture. We extended the study for a realistic ternary mixture SO_2, CO_2, and N_2, for which the selectivity of SO_2 over CO_2 is found to be maximum for the COOH functionalized GNR. In addition, the selectivity of SO_2 over N_2 is higher than that of CO_2 over N_2 in all functionalized GNRs.

SUPPLEMENTARY MATERIAL

See supplementary material for additional snapshots of adsorption in CH_3, NH_2, and OH functionalized GNRs, in addition to Fig. 5. Snapshot of ternary mixture adsorption is also given.

ACKNOWLEDGMENTS

We wish to acknowledge the Ministry of Earth Sciences, Government of India. The computational facility is provided by HPC, Computer Center, Indian Institute of Technology Kanpur, India.

[1] Z. Zhang, Z.-Z. Yao, S. Xiang, and B. Chen, Energy Environ. Sci. **7**, 2868 (2014).
[2] M. Rahimi, J. K. Singh, D. J. Babu, J. J. Schneider, and F. Mller-Plathe, J. Phys. Chem. C **117**, 13492 (2013).
[3] A. Sayari, Y. Belmabkhout, and R. Serna-Guerrero, Chem. Eng. J. **171**, 760 (2011).
[4] B. G. Miller, *Fossil Fuel Emissions Control Technologies: Stationary Heat and Power Systems* (Butterworth-Heinemann, 2015).
[5] B. He, X. Zheng, Y. Wen, H. Tong, M. Chen, and C. Chen, Energy Convers. Manage. **44**, 2175 (2003).
[6] A. M. Strömberg and H. T. Karlsson, Chem. Eng. Sci. **43**, 2095 (1988).
[7] M. H. H. van Dam, A. S. Lamine, D. Roizard, P. Lochon, and C. Roizard, Ind. Eng. Chem. Res. **36**, 4628 (1997).
[8] R. Deng, L. Jia, Q. Song, S. Su, and Z. Tian, J. Hazard. Mater. **229**, 398 (2012).
[9] C. Chen, Z.-G. Tang, C.-C. Zhou, Ind. Eng. Chem. Res. **43**, 6714 (2004).
[10] J. Boniface, Q. Shi, Y. Li, J. Cheung, O. Rattigan, P. Davidovits, D. Worsnop, J. Jayne, and C. Kolb, J. Phys. Chem. A **104**, 7502 (2000).
[11] C. Wang, G. Cui, X. Luo, Y. Xu, H. Li, and S. Dai, J. Am. Chem. Soc. **133**, 11916 (2011).
[12] D. Yang, M. Hou, H. Ning, J. Ma, X. Kang, J. Zhang, and B. Han, ChemSusChem **6**, 1191 (2013).
[13] J. Guo and A. C. Lua, J. Colloid Interface Sci. **251**, 242 (2002).
[14] B. Grzyb, A. Albiniak, E. Broniek, G. Furdin, J. March, and D. Bgin, Microporous Mesoporous Mater. **118**, 163 (2009).
[15] W. Wang, X. Peng, and D. Cao, Environ. Sci. Technol. **45**, 4832 (2011).
[16] M. Rahimi, D. J. Babu, J. K. Singh, Y.-B. Yang, J. J. Schneider, and F. Müller-Plathe, J. Chem. Phys. **143**, 169901 (2015).
[17] A. Srinivasan and M. W. Grutzeck, Environ. Sci. Technol. **33**, 1464 (1999).
[18] E. Ivanova and B. Koumanova, J. Hazard. Mater. **167**, 306 (2009).
[19] X. Wang, X. Ma, S. Zhao, B. Wang, and C. Song, Energy Environ. Sci. **2**, 878 (2009).
[20] L. Xu, J. Guo, F. Jin, and H. Zeng, Chemosphere **62**, 823 (2006).
[21] I. Mochida, Y. Korai, M. Shirahama, S. Kawano, T. Hada, Y. Seo, M. Yoshikawa, and A. Yasutake, Carbon **38**, 227 (2000).
[22] C. A. Fernandez, P. K. Thallapally, R. K. Motkuri, S. K. Nune, J. C. Sumrak, J. Tian, and J. Liu, Cryst. Growth Des. **10**, 1037 (2010).
[23] S. Yang, J. Sun, A. J. Ramirez-Cuesta, S. K. Callear, W. I. David, D. P. Anderson, R. Newby, A. J. Blake, J. E. Parker, C. C. Tang *et al.*, Nat. Chem. **4**, 887 (2012).
[24] F. Marsh and H. Rodriguez-Reinoso, *Activated Carbon* (Elsevier Science, Oxford, 2006).
[25] H. Deng, C. J. Doonan, H. Furukawa, R. B. Ferreira, J. Towne, C. B. Knobler, B. Wang, and O. M. Yaghi, Science **327**, 846 (2010).
[26] P. B. Malla and S. Komarneni, J. Porous Mater. **1**, 55 (1995).
[27] V. S. Kandagal, A. Pathak, K. Ayappa, and S. N. Punnathanam, J. Phys. Chem. C **116**, 23394 (2012).
[28] P. Halder, M. Maurya, S. K. Jain, and J. K. Singh, Phys. Chem. Chem. Phys. **18**, 14007 (2016).
[29] J. Kong, M. G. Chapline, H. Dai *et al.*, Adv. Mater. **13**, 1384 (2001).
[30] K. S. Novoselov, A. K. Geim, S. V. Morozov, D. Jiang, Y. Zhang, S. V. Dubonos, I. V. Crigorieva, and A. A. Firsov, Science **306**, 666 (2004).
[31] F. Schedin, A. K. Geim, S. V. Morozov, E. W. Hill, P. Blake, M. I. Katsnelson, and K. S. Novoselov, Nat. Mater. **6**, 1476 (2007).

[32]T. Wehling, K. Novoselov, S. Morozov, E. Vdovin, M. Katsnelson, A. Geim, and A. Lichtenstein, Nano Lett. **8**, 173 (2008).
[33]O. Leenaerts, B. Partoens, and F. M. Peeters, Phys. Rev. B **77**, 125416 (2008).
[34]B. Huang, Z. Li, Z. Liu, G. Zhou, S. Hao, J. Wu, B.-L. Gu, and W. Duan, J. Phys. Chem. C **112**, 13442 (2008).
[35]Y. Houndonougbo, "Molecular simulation of carbon capture in a series of isoreticular zeolitic imidazolate materials," in *ACS Symposium Series* (American Chemical Society, 2013), pp. 83–98.
[36]J.-S. Bae and S. K. Bhatia, Energy Fuels **20**, 2599 (2006).
[37]P. Kowalczyk, H. Tanaka, K. Kaneko, A. P. Terzyk, and D. D. Do, Langmuir **21**, 5639 (2005).
[38]A. Kumar, R. F. Lobo, and N. J. Wagner, AIChE J. **57**, 1496 (2011).
[39]X. Peng, D. Cao, and J. Zhao, Sep. Purif. Technol. **68**, 50 (2009).
[40]G. K. Dimitrakakis, E. Tylianakis, and G. E. Froudakis, Nano Lett. **8**, 3166 (2008).
[41]T. A. Makal, J.-R. Li, W. Lu, and H.-C. Zhou, Chem. Soc. Rev. **41**, 7761 (2012).
[42]A. Gotzias, H. Heiberg-Andersen, M. Kainourgiakis, and T. Steriotis, Carbon **49**, 2715 (2011).
[43]A. Sharma, S. Namsani, and J. K. Singh, Mol. Simul. **41**, 414 (2015).
[44]M. H. Ketko, G. Kamath, and J. J. Potoff, J. Phys. Chem. B **115**, 4949 (2011).
[45]J. J. Potoff and J. I. Siepmann, AIChE J. **47**, 1676 (2001).
[46]T. Dasgupta, S. N. Punnathanam, and K. Ayappa, Chem. Eng. Sci. **121**, 279 (2015).
[47]G. Maitland, M. Rigby, E. Smith, and W. Wakeham, *Intermolecular Forces: Their Origin and Determination* (Oxford University Press, 1981).
[48]E. Mostaani, N. D. Drummond, and V. I. Fal'ko, Phys. Rev. Lett. **115**, 115501 (2015).
[49]P. Ungerer, B. Tavitian, and A. Boutin, *Applications of Molecular Simulation in the Oil and Gas Industry: Monte-Carlo Methods* (Editions TECHNIP, 2005).
[50]D. Frenkel and B. Smit, *Understanding Molecular Simulation*, 2nd ed. (Academic Press, 2002).
[51]E. Lemmon, M. McLinden, and D. Friend, NIST Chemistry Webbook, NIST Standard Reference Database No. 69, NIST, 2005.
[52]S. J. Mahdizadeh and S. F. Tayyari, Theor. Chem. Acc. **128**, 231 (2011).
[53]D. D. Do and H. D. Do, J. Phys. Chem. B **110**, 17531 (2006).
[54]A. L. Myers and P. A. Monson, Langmuir **18**, 10261 (2002).
[55]T. Vuong,, and P. A. Monson, Langmuir **12**, 5425 (1996).
[56]D. Nicholson, *Computer Simulation and the Statistical Mechanics of Adsorption* (Academic Press, 1982).
[57]D. J. Babu, F. G. Kuhl, S. Yadav, D. Markert, M. Bruns, M. J. Hampe, and J. J. Schneider, RSC Adv. **6**, 36834 (2016).
[58]M. Molina-Sabio, A. Muecas, F. Rodrguez-Reinoso, and B. McEnaney, Carbon **33**, 1777 (1995).
[59]Y.-H. Zhang, Y.-B. Chen, K.-G. Zhou, C.-H. Liu, J. Zeng, H.-L. Zhang, and Y. Peng, Nanotechnology **20**, 185504 (2009).
[60]A. Ahlam, G. H. Ismail, A. M. Babeer *et al.*, J. Surf. Eng. Mater. Adv. Technol. **3**, 287 (2013).
[61]X. Zhou, W. Huang, J. Miao, Q. Xia, Z. Zhang, H. Wang, and Z. Li, Chem. Eng. J. **266**, 339 (2015).
[62]Z. Zhang, S. Huang, S. Xian, H. Xi, and Z. Li, Energy Fuels **25**, 835 (2011).
[63]J. A. Campbell, J. Chem. Educ. **62**, 231 (1985).
[64]K. Foo and B. Hameed, Chem. Eng. J. **156**, 2 (2010).
[65]R. D. Johnson, "Computational chemistry comparison and benchmark database release 17b standard reference," Database number- 101, 2015.
[66]M. Rahimi, J. K. Singh, and F. Müller-Plathe, Phys. Chem. Chem. Phys. **18**, 4112 (2016).